PMMA composite bone cement containing bioactive and ferrimagnetic glass-ceramic particles: Effect of temperature and of the additional phase on some physical and

Ceramics International 49 (2023) 24885–24894

Contents lists available at ScienceDirect

Ceramics International

journal homepage: www.elsevier.com/locate/ceramint

PMMA composite bone cement containing bioactive and ferrimagnetic glass-ceramic particles: Effect of temperature and of the additional phase on some physical and mechanical properties

Marta Miola [a], Fabrizio Barberis [b], Alberto Lagazzo [b], Enrica Vernè [a,*]

[a] Department of Applied Science and Technology, Politecnico di Torino, C.so Duca degli Abruzzi 24, 10129, Torino, Italy
[b] Department of Civil, Chemical and Environmental Engineering, University of Genoa, via all'Opera Pia 15, 16145, Genoa, Italy

ARTICLE INFO

Handling Editor: Dr P. Vincenzini

Keywords:
B. Composites
C. Mechanical properties
D. Glass ceramics
E. Biomedical applications
Hyperthermia

ABSTRACT

In this work, PMMA-based composite bone cements, embedding bioactive and ferrimagnetic glass-ceramic particles, have been prepared and characterized. Bioactivity, wettability, density, curing parameters, viscoelastic behaviour, bending strengths and creep have been investigated at 37 °C. The growth of a layer of HA on the samples surface after immersion in SBF has been confirmed. The presence of glass-ceramic particles improved the wetting behaviour of the composite cements. Shorter curing times and lower maximum temperatures for the three composite cements, in comparison to the plain one, have been detected. Almost unaffected mechanical properties of the composite bone cements have been found in comparison to those of the plain commercial cement both at room and at 37 °C. A little increase of the viscous flow has been evidenced in the composite samples at 37 °C. Radiographic imaging confirmed the intrinsic radiopacity of the composite cements.

1. Introduction

Hyperthermia is recognised as an effective practice for tumors treatment, in synergy with traditional therapies, such as surgery, chemotherapy and radiotherapy [1,2]. In particular, magnetic induction hyperthermia has been studied in recent years as a novel approach to bone tumor treatment [3]. It uses an external alternating magnetic field to stimulate magnetic materials implanted in the body's tissues, for example into the cavity created by a tumor removal, to generate controlled heat. The implanted materials possess magnetic properties that, through hysteresis losses, produce controlled heating, generally up to a temperature in the range between 41 °C and 43 °C, to destroy cancer cells [4]. The reached temperature depends on materials properties, intensity and frequency of the applied magnetic field, as well as on the bone tissue density [4]. This method is targeted at the tumor site, preserving the nearby healthy tissues and can be applied to treat a variety of solid tumors [3,4]. Ferrimagnetic bone cements are promising materials for applications in hyperthermia [5–7] when large local excision surgery of the metastatic bone and its protection from tumors-associated pathological fractures are necessary. Bone tissue substitution and regeneration is often approached, beside other materials, with bioactive glasses and glass-ceramics that, when implanted, are able to induce the growth of a hydroxyapatite layer on their surface, thus stimulating the formation of new tissue and creating a chemical bond with bone [8,9]. A bioactive ferrimagnetic glass-ceramic belonging to the system SiO_2–Na_2O–CaO–P_2O_5–FeO–Fe_2O_3 (SC45), has been developed by Bretcanu et al. [10,11]. This material exhibited controlled bioactivity kinetics, good magnetic and thermal properties, cytocompatibility, and it was efficaciously functionalized with antineoplastic agents [12–15]. The SC45 glass-ceramic has been successfully used in previous works to load a PMMA-based commercial bone cement obtaining a new class of composite bone cements with both bioactive and ferrimagnetic properties [16–18].

In the previous papers the bone cement loaded with SC45 glass-ceramic has been fully characterized for its bioactivity, magnetic properties, heating ability *in vitro*, modelling of heating ability *in vivo*, safety (cytocompatibility), efficacy (selective induction of tumoral cell death), as well as on its mechanical behaviour at room temperature. In literature, several studies have been reported about other kinds of composite bone cements (without ferromagnetic phases), usually investigating the effect on the mechanical properties of the addition of radio-opacizers, antibacterial phases or reinforcing phases [19–25], but very few studies reports the effect of temperature on the properties of acrylic cements [26]. However, in the human body environment, to which the

* Corresponding author.
E-mail address: enrica.verne@polito.it (E. Vernè).

https://doi.org/10.1016/j.ceramint.2023.05.017
Received 9 March 2023; Received in revised form 11 April 2023; Accepted 2 May 2023
Available online 5 May 2023

bone cement is exposed, several parameters are different from the laboratory condition ones, among other, the temperature. Moreover, the effect of temperature could be dissimilar on plain acrylic matrix and in the acrylic composite cement containing a glass-ceramic phase, due to potential differences in the material density or due to the presence of creep at the interface between the glass-ceramic particles and the acrylic matrix. Finally, it is important to verify if the composite bone cement, containing a ferrimagnetic phase, is still observable with the most common imaging techniques.

The present paper is focused on the characterization of the composite bone cement containing the SC45 glass-ceramic, considering the above-mentioned issues. After a preliminary investigation of some physical properties (wettability and density) and of the setting parameters, which could be affected by the addition of the SC45 particles, the mechanical properties of the composite cement have been investigated at the operating temperature of 37 °C, considering this temperature as the ordinary condition of use of the implant, planning the study at the therapeutic conditions (i.e. 41 °C – 43 °C for cycles of few minutes) in future investigations. In particular this study has been dedicated to the analysis of the viscoelastic behaviour, the bending and compressive strengths, and on creep phenomena.

Composite bone cements samples loaded with 45S5 has been also subjected to radiography and magnetic resonance imaging (MRI) with the purpose to assess the most suitable imaging technique for *in vivo* clinical follow up.

2. Materials and methods

2.1. Synthesis of composite cements

The composite cements were synthesized by loading different percentage in weight (10, 15 and 20 wt%) of a bioactive and ferrimagnetic glass-ceramics (SC45) to a commercial poly(methyl methacrylate) PMMA-based cement with medium viscosity (Palamed®, produced by Heraeus Kulzer S.r.l.). Briefly, the SC45 composition is reported in Refs. [10,14], it contains magnetite crystals embedded in a bioactive amorphous phase with the same oxides ratio as the Hench bioactive glass (45S5). The glass-ceramic frit was prepared by melting and quenching process; then it was ball milled and sieved below 20 μm to obtain powders. The composite cements will be named, from now on, with the acronyms P10, P15 and, P20, in reference to the wt% of SC45. The three percentages of SC45 powders have been selected on the base of previous results [16–18] and mixed with the solid phase of the bone cement Palamed®, produced by Heraeus Kulzer S.r.l., a mixture of poly-(-methylacrylate, methylmethacrylate), ZrO_2 as radio-opaque phase, benzoyl-peroxide, colorant E141 (named simply PMMA from now on). The blend of solid phases (PMMA + SC45 powders) was then mixed with the liquid one, containing methyl methacrylate, *N*,*N*-dimethyl-p-toluidine, hydroquinone, colorant E141 (named simply MMA from now on) using the solid phase (PMMA + SC45)/liquid phase (MMA) ratio of 2 g/mL, as suggested by the producer for plain Palamed®.

2.2. Composite bone cements characterization

2.2.1. Bioactivity

The bioactivity of the composites has been deeply investigated in previous works [16,17]. In the present paper the bioactivity of the samples has been repeated to assess its reproducibility by following the well-known Kokubo's protocol [27] for *in vitro* test in simulated body fluid (SBF), used in literature to evaluate the surface reactivity of bioactive glasses and glass-ceramics during interaction with the biological fluids [28–30]. As reported in Refs. [16,17] each composite cement (P10, P15, P20) was soaked in 25 mL of SBF at 37 °C for four weeks. Every three days the solution was refreshed under pH control. At the end of the test, samples have been removed from the SBF, rinsed in distilled water, dried at room temperature and characterized by scanning electron microscopy (SEM–FEI, QUANTA INSPECT 200) and energy dispersion spectrometry (EDS–EDAX PV 9900).

2.2.2. Physical properties

2.2.2.1. Contact angle (CA). The static CA was measured on rectangular bars of 37 mm × 10 mm and 3.3 mm. The surface was previously cleaned with acetone and then washed with demineralized water and finally dried in air at room temperature. The test, based on the sessile drop method, consists in the determination of the geometrical angle formed between the solid sample's surface (solid/liquid interface) and the tangent of the droplet's shape at the edge of the droplet (gas/liquid interface). The profile of a deionized water drop of about 15 mg was acquired with a USB DinoLight microscope and elaborated with AutoCAD for the determination of the CA.

2.2.2.2. Apparent density. Apparent density was calculated using the gravimetric and Bouyancy Method based on Archimedes's principle. As samples were used specimens consisting in cylinders of 6 mm in diameter and 12 mm in height. As auxiliary liquid was used demineralized water at room temperature.

2.2.2.3. Curing parameters. The measure of the variations in the temperature occurring in PMMA bone cements during the exothermic curing process is commonly used to evaluate the four phases of the polymerization: mixing, dough, working and setting time [31]. In a previous paper [18], the determination of the setting time of the composite bone cements has been carried out following the ISO 5833(2002) standard [32], and any significant difference among all the composite cements in comparison with the plain commercial one has been assessed. In the present paper, for a better comparison between the composite and commercial cement, the curing parameters have been investigated as described below. Four different composite cements with 0 wt%, 10 wt, 15 wt% and 20 wt% of SC45 glass-ceramic were prepared. Powders of Palamed® and SC45 glass-ceramic were manually mixed for 30 min, then the liquid phase (containing the MMA monomer) was added by means of a micropipette, and mixed for 30 s, up to the beginning of the polymerization reaction, maintaining the same ratio between polymer and monomer of the commercial formulation.

The curing parameters were evaluated with the DMA apparatus described in the 2.2.3 section concerning the mechanical characterization, consisting of a cylindrical indenter of 5 mm in diameter, connected with a force transducer and immersed for 2 mm in the cement paste contained in a cylinder of Teflon of 20 mm in diameter. The test was run with a frequency in the range between 5 Hz and 5.25 Hz accordingly to each sample features. The evolution of the storage modulus E' vs. the time is strictly connected with the increasing of the stiffness of the cement mixture and therefore with the advancing of the polymerization reaction. A thermocouple was positioned in contact with the sample to monitor the temperature evolution during the curing process.

2.2.3. Mechanical properties at 37 °C

2.2.3.1. Three points bending test. The measurements were carried out at 37 °C on rectangular bars of 37 mm × 10 mm and 3.3 mm, by using a Zwick/Roell Z10 universal electromechanical machine. The fixture consists of two roller support of 5 mm in diameter, set at a distance of 30 mm on which is lent the sample. The bending is induced by a third pin of the same diameter and geometry as the others two moving downward with a rate of 1 mm/min. To assure the thermal stability of the sample the specimen was maintained at 37 °C in a thermostatic bath for 5 min before the test. All the tests are repeated four times for each formulation of cement. The fracture surfaces after bending test have been observed, in order to explore the fracture mechanism.

2.2.3.2. Complex modulus. Dynamic flexural Analysis (DMA) were carried out the same rectangular bars of 37 mm × 10 mm and 3.3 mm used for the static 3 points bending.

The test was performed using a prototype DMA apparatus, consisting of a mini-shaker operating in a range between 1 Hz and 10 KHz with maximum force of 1.5 N, a Laser vibrometer to measure the displacement, set at 80 μm/V and a force transducer. All the devices were connected to a PC through an NI acquisition card and the signals were elaborated by mean a LabView program. The sample were placed on two roller support of 5 mm in diameter, with a span of 30 mm, directly connected with the shaker, while a cylindrical pin of 5 mm in diameter, fixed to the force transducer was approached until touching the upper surface of the sample and then a pre-strain was applied. A 10% strain was considered to evaluate the stiffness of the external layers and the response of the system at low solicited conditions, a 20% strain to check the internal bulk, but without inducing a damage of the internal structure. The test was run with an oscillation between 2 Hz and 100 Hz and the sinusoidal signal of the displacement and of the force, respectively response and stimulus, was elaborated by the software producing a spectrum containing the storage modulus (E') and the loss modulus (E") vs. the frequency. Al the tests were performed at 37 °C.

2.2.3.3. Creep. Creep test was performed on rectangular bars of 37 mm × 10 mm and 2 mm of three types of cement (Palamed®, P10 e P20). The samples were submitted to a constant stress of 15 MPa for 100 h in 3 points bending configuration, by applying a load of 3 Kgf. This value was chosen considering a stress, during the operating conditions *in vivo*, estimated in the range 2–11 MPa [33].

The apparatus employed for the creep test consists of a vessel in polycarbonate containing water maintained at 37 °C through a thermostatic bath and circulating by means of a pump. The inflection of the samples immersed in the water was measured continuously through a LVDT and recorded with a computer. To avoid the formation of organic microorganisms Amoxicillin antibiotic was dispersed into the bath.

2.2.4. Imaging

2.2.4.1. Radiopacity. In order to investigate the intrinsic radio-opacity of the glass-ceramic blended in the polymeric matrix, some composite bone cement samples, containing 20 wt% of glass-ceramic powders, were also prepared without including the radio-opaque agent. These samples were then subjected to radiography, as reported in a previous work [34].

2.2.4.2. Magnetic resonance imaging (MRI). In order to assess if the use of MRI can be recommended to visualize the implants into in the body, discs of bone cements (60 mm diameter and e 5 mm high) of plain Palamed® (as control), P10, P15 and P20 were placed on the top of a cylindrical phantom containing water as contrast agent. The cylinder contains some reference rigid structure of standard geometry useful to assess eventual deformations, during the MR scan, as reported in Fig. 1.

The O-Scan system (ESAOTE S.p.A), consisting of an MRI apparatus for limbs diagnosis (knee, ankle, calf, wrist, elbow) was used to perform the scan. The apparatus generates a constant magnetic field of intensity equal to 0.31 T, thanks to the presence of a permanent magnet. The magnet housing was kept at a constant temperature, with a control performed by a special software in the order of mK, as the orientation of the magnetic moments of the magnet, and consequently its magnetization, are strongly dependent on the temperature. In this way, a magnetic field as constant as possible was generated, the intensity of which did not depend on the temperature variations in the analysis room. Furthermore, the O-Scan machine was positioned inside a Faraday cage, which acts as a magnetic shield from any external signals that could affect the diagnostic quality of the investigation. The oscillating field, applied with a frequency of 13 MHz by a second electromagnet, generated the MRI signal for Free Induction Decay (FID) which was sent to an acquisition card and finally processed by a self-built software. For each sample positioned on the phantom surface, 18 images were collected, each depicting a different section of the system under analysis.

3. Results and discussion

3.1. Bioactivity

The structure, morphology and the bioactive behaviour of the composite cements were estimated in previous works [16,17], evidencing a good dispersion of the bioactive and magnetic glass-ceramic in the polymeric matrix. The *in vitro* test in simulated body fluid (SBF, Kokubo protocol [29]) performed in the present work confirmed the ability of the composite cements to induce the precipitation of hydroxyapatite on their surface after 28 days of immersion in SBF. Fig. 2 shows, as an example of this behaviour, the P15 morphology (Fig. 2a) and SEM/EDS analysis of P15 before and after 4 weeks of SBF soaking (Fig. 2b and c respectively). In detail, Fig. 2 a shows the sample not soaked in SBF, with the SC45 particles (where the magnetite crystals embedded in the glassy matrix are visible) dispersed in the PMMA matrix, together with the zirconia particles (the radio-opacifier agent). Fig. 2b and 2c demonstrated the precipitation of agglomerate rich in Ca and P on the composite surface.

3.2. Physical properties

3.2.1. Contact angle

Fig. 3 reports the results of the wettability test, including the images of the sessile droplet on the various samples and the CA values. The CA measurements for the four different composite cements highlight that the presence of the ceramic increases the wettability of the water-

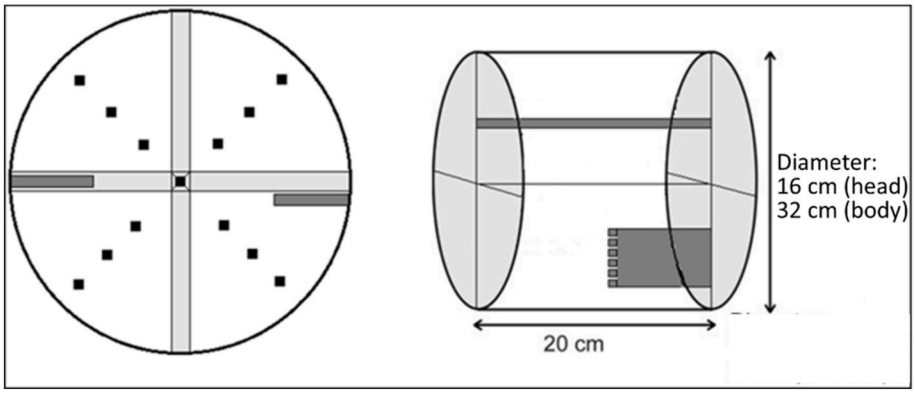

Fig. 1. Schematic view of the cylindrical phantom with reference rigid structures.

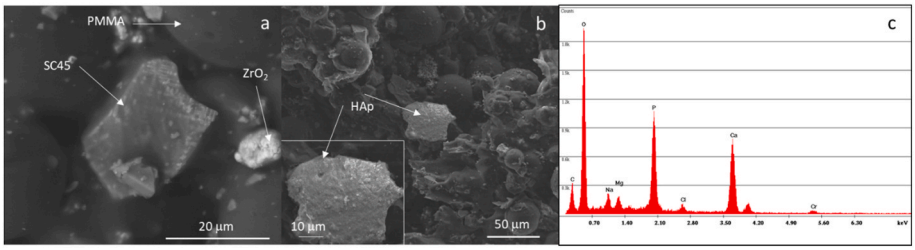

Fig. 2. P15 micrography (a) and SEM/EDS analysis of P15 after 4 weeks of soaking in SBF (b, c).

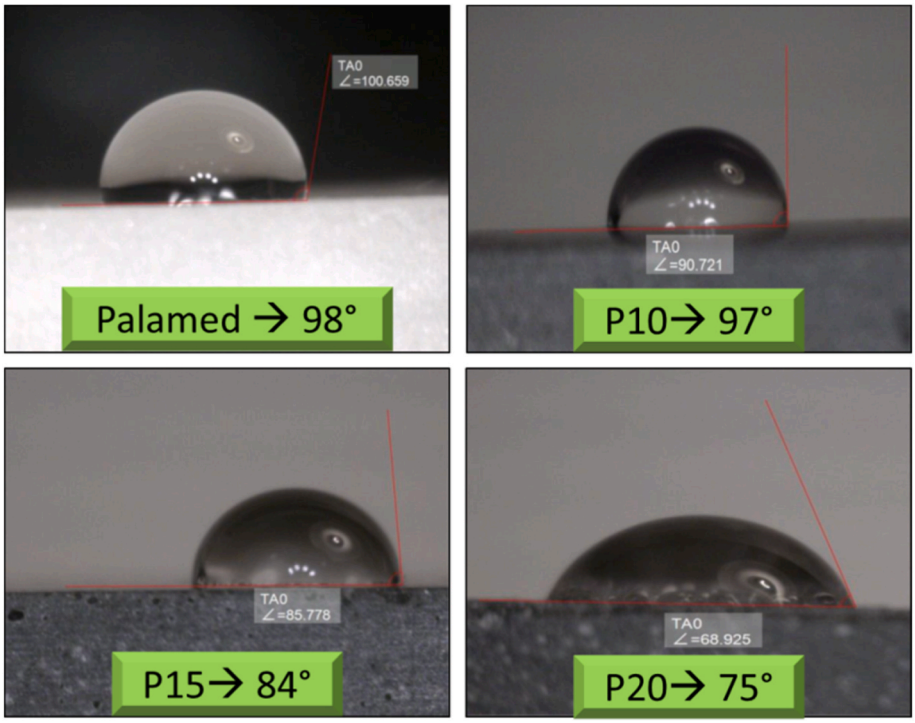

Fig. 3. Analysis of wettability.

samples systems due to the higher surface energy of the ceramic and therefore a more evident hydrophilicity (i.e. lower CA) with respect of the polymeric substrate. The values calculated as mean of three measurements, read a CA = 101.5° for the Palamed® cement without filler and 95.2°, 84.6° and 76.4° for the composite with 10 wt%, 15 wt% and 20 wt% of SC45 respectively. These data sustain the hypothesis that the presence of the ceramic glass might lead to higher bioactivity of these composites with respect to the pure Palamed® cement. This is a quite important result due to the fact that filler percentages higher than 10% turn the water-solid behaviour from non-wetting to a wetting one, greatly affecting the overall materials interactions and adhesion properties in the biological environment. As reported in literature [35,36], hydrophilic surfaces can promote the growth, the mineral deposition and the differentiation of osteoblast-like cells, such as MG63 and hFOB, compared to hydrophobic surfaces.

3.2.2. *Apparent density*

The densities of the different samples are reported in Table 1. The results evidence the density increase with a linear trend, due to the addition of the glass-ceramic particles to the polymeric matrix. The comparison with the theoretical values, calculated with the mixing rule, evidences a low deviation of the experimental values, assessing a few porosity increase with the increase of the glass ceramic particles amount, as expected due to the manual mixing.

Table 1
Density measurements by means of Archimedes' principle and rule of mixtures.

	Archimedes' principle	Theoretical Density
Palamed®	1.16 ± 0.01	1.16
P10	1.22 ± 0.02	1.27
P15	1.24 ± 0.01	1.32
P20	1.28 ± 0.02	1.38

3.2.3. *Curing parameters*

Fig. 4 shows the E′ modulus (a) and temperature (b) trends vs time obtained by means of dynamo-mechanical analysis. The value considered to identify the working time of the cement is the maximum in the curve E′ vs. time (Fig. 4a), that represents the point over that the indenter detaches the surface of the specimen. This fact occurs when the stiffness of the cement becomes too high to permit that the sample adapts to the movement induced by the shaker. It should be underlined that the working time measured with this apparatus does not completely overlap with the working time measurable by the method described by the ISO standard, but can be related to it. The trend reported in Fig. 4 a reveals an increase of E′ modulus and a shortening of the needed time to reach the maximum value of E' (from 7′ 42″ to 4′ 57″), i.e. a shortening of the working time, as a function of the amount of glass-ceramic particles. Moreover, a marked difference was detected between the plain

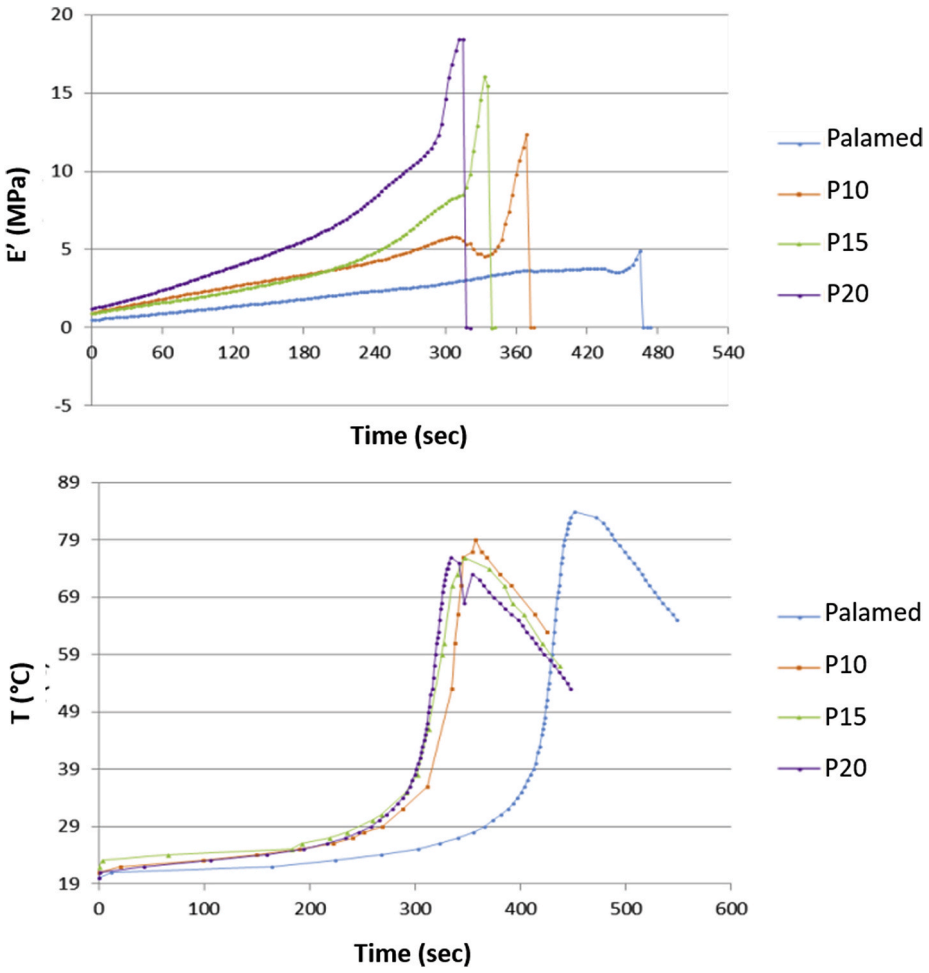

Fig. 4. Elastic modulus (a) and temperature (b) trends vs time obtained by means of dynamo-mechanical analysis.

Palamed® and the composite cements. This difference is more evident in the temperature trends (Fig. 4b), that show shorter curing times and lower maximum temperature (T peak) for the three composite cements in comparison to the plain one.

The values of T peak and working time (i.e. the time needed to reach the E' max) are also reported in Table 2. These results are partially in disagreement with those previously reported in literature [18] and can be explained with the different experimental setup used in this work, which measures more precisely the viscous behaviour of the polymeric matrix and could evidence any differences between pure bone cement and the composite ones.

3.3. Mechanical properties at 37 °C

3.3.1. Three points bending test

The presence of glass-ceramic particles induces an embrittlement of the cement with a reduction of the ultimate flexural stress both at room temperature [16] and at 37 °C (Table 3). The embrittlement could also be related to the presence of few porosity, as assessed by the density measurement (Table 1). A concentration of 20 wt% of SC45 shows a measured flexural stress of 47,7 ± 3 and 45,7 ± 1,5 MPa at T_{room} and 37 °C respectively, and these values are below the lower limit of 50 MPa fixed for bone cement by the standard ISO 5833–2002. Due to this fact, this concentration must be considered as the maximum limit to produce suitable bone cements.

Fig. 5 reports as an example of fracture surface, the plain Palamed® and the P10 specimens after the fracture at T_{room} and 37 °C, respectively. Some cleavage surfaces are evident, due to the intrinsic brittle behaviour of PMMA, both on the plain Palamed® and on the P10 samples, in the samples tested at T_{room} and 37 °C. In all the samples the ZrO_2 particles (i.e. the radiopaque phase) are exposed, as well as the SC45 particles in the composite cements. The few differences in the behaviour at T_{room} and 37 °C are not perceptible from a morphological point of view.

3.3.2. Complex modulus

As can be observed in Fig. 6 a, the elastic modulus at room

Table 2
Time to reach the maximum value of E' and maximum temperature of commercial Palamed® and P10, P15, P20 composite cements.

Sample	Time to reach the E′ max (min)	T max (°C)
Palamed®	7′ 42″	84
P10	5′ 57″	79
P15	5′ 27″	76
P20	4′ 57″	76

Table 3
Mechanical properties of the different cement formulations at room temperature [16] and 37 °C.

	Bending σ [MPa]	
Temperature	Room T	T = 37 °C
Palamed®	58,4 ± 2,4	54,7 ± 2,1
P10	51,5 ± 3	56,5 ± 3,7
P15	50,1 ± 2,5	48,5 ± 2,2
P20	47,7 ± 3	45,7 ± 1,5

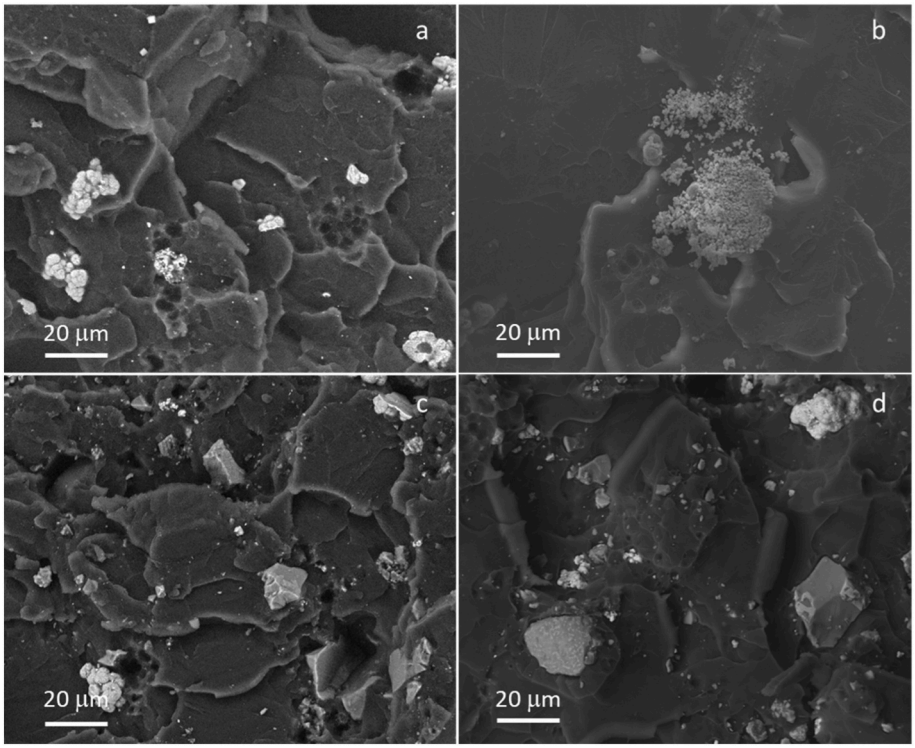

Fig. 5. *Micrography of the fracture surfaces of plain Palamed®* (a, b) *and P10 composite bone cement (c, d) after three points bending test at room temperature* [16] *(b, d) and 37°C (a, c).*

temperature of the composites increases with the increasing of the oscillating frequency until a plateau over 30 Hz, independently of the SC45%. The amount of the SC45 shows a growth of the storage modulus from 2600 MPa, cement without glass ceramic, to 3500 MPa, cement with 20 wt% of glass ceramic, with an increase more evident between 15 wt% and 20 wt% with respect to the low concentrations. The tests carried out at 37 °C (Fig. 6b) do not evidence differences for the plain cement (blue curve), while display lower values for the composite formulations, with a reduction of about 12% for P20 (3100 MPa vs. 3500 MPa) and a storage modulus of the P15 (orange plot) slightly lower than the one of the P10 (grey plot). The loss factor, $Q^{-1} = E''/E'$, plotted in Fig. 7, does not show differences among the samples with and without SC45, both at room temperature and at 37 °C, but just an increase from 0.08 (at room temperature) to 0.10 (at 37 °C) due to softening induced by the high value of temperature.

3.3.3. Creep

The displacement of the sample vs. the time increases gradually without reaching any plateau within the 100 h of the test (Fig. 8) so we can assume that all the samples reached the secondary steady-state creep stage, where the strain rate is constant. In details, during the first 10 h all the samples show the same behaviour with a fast-initial rise of the curves. Afterwards, the pure cement shows a different displacement in comparison with the composite samples, since at the end of the test it reads 0.9 mm, thus about 50% lower than the composite with 20% of glass ceramic, that at 100 h reaches a deflection of 1.5 mm. This trend can be related to different factors. First, the composite samples present a certain degree of porosity as a function of the glass ceramic particles amount (as discussed above considering the density values reported in Table 1), that can fasten the viscous flow of the polymeric matrix. Moreover, the creep test was performed in solution, so a partial dissolution of the glass ceramic particles could occur, inducing the generation of further porosities as well as a gradual softening of the polymeric matrix. These results are in accordance with the reduction of the storage modulus observed for the composite samples at 37 °C, much more evident with increase of the glass ceramic particle amount (Fig. 6).

3.4. Imaging

3.4.1. Radiopacity

The possibility of making visible bone implants after surgery by the current imaging techniques is fundamental in view of the final application. However, imaging of tissues nearby to the magnetic implants is very challenging. The most common techniques are X-ray Imaging (XR) Computed Tomography (CT) and the Magnetic Resonance Imaging (MRI). The introduction of SC45 glass ceramic particles into the PMMA-based bone cements should not hamper the possibility of a post-surgical follow up of the new composite bone cements with at least one of the above-mentioned imaging techniques. In principle, the presence of iron oxides into the glass-ceramic could be exploited for XR imaging, if no image deformation occurs. Nevertheless, some materials with magnetic response can originate an artefact in MRI images [37], thus a further characterization with this technique it is also of interest.

The radio-opacity of the reference (with and without radiopaque phase) and of the composite cement containing SC45 powders (without radiopaque phase) is reported in Fig. 9. As can be observed, the presence of the glass-ceramic does not induce any image deformation and, at the same time, imparts radio-opacity to the PMMA-based cement, comparable with commonly used radiopaque phases, as also assessed by Micro computed tomography (micro-CT) in a previous work [16].

The possibility of reducing or removing of the radiopaque phase, habitually used in the commercial bone cements, is considered an added value, in view of the improvement of their mechanical strength, as reported in literature [38–40]. Moreover, it was stated that the commonly used radiopaque agents may have a role in bone resorption [41]. Therefore, the partial or total substitution of inert radiopaque phases with a bioactive glass-ceramic with intrinsic radio-opacity could be a way to limit the worsening of the mechanical properties and, at the same time, to improve the osteointegration ability of the bone cement. These results suggest that X-ray Imaging (as well as Computed Tomography

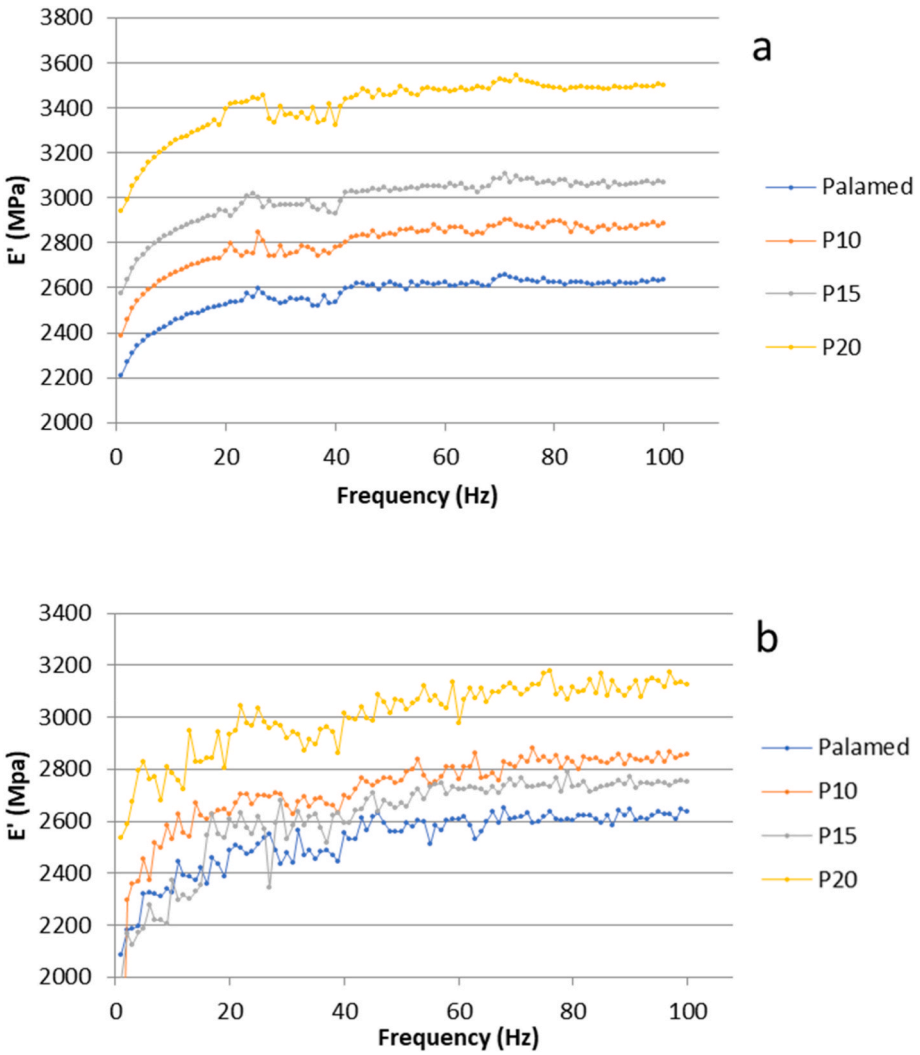

Fig. 6. Storage modulus E′ evaluation by means of DMA at room temperature (a) and at 37 °C (b).

previously investigated) can be recommended for the surgical follow-up of a bone cement containing a ferrimagnetic glass ceramic in the amount investigated in this work.

3.4.2. *Magnetic resonance imaging*

The *spin-echo* scans allowed the acquisition of MR images of plain Palamed®, P10, P15 and P20 samples. The scans, weighted both on T_1 and T_2, have been performed on 18 sections of the phantom containing contrast liquid, and during each analysis the bone cement sample has been placed on the phantom surface. In Fig. 10 the results obtained with the plain Palamed® samples are reported. In detail, only the images obtained in the central section of the phantom have been reported, since they are representative of all the images obtained at different distances from the surface. The plain Palamed® sample is not visible since it does not have a magnetic response, but as evidenced by the picture, its presence does not affect the image acquisition of the reference structures, as they appear not deformed. Moreover, neither haloes nor lateral deformations, due to the interference of the material with the signal emission, are visible. Furthermore, no differences between the images weighted on T_1 and T_2 are evident, as a consequence of the absence of tissues of different densities, as happens, on the contrary, in the human body.

Fig. 11 reports the results obtained with the P10 (a-h), P15 (i-p) and P20 (q-z) samples on the phantom in different sections starting from surface to the central one. In this case the presence of the sample on the phantom surface causes a strong distortion of the images: in the surface sections, a dark halo is visible, and the image becomes more and more deformed from the surface to the central sections, as long as both the guide structures and the original shape of the phantom are no longer distinguishable. In fact, it has been reported that large and rapidly switched magnetic field gradients could induce eddy currents in electrically conductive materials introduced into the MR scanner, that, in turn, could cause additional unwanted, rapidly and slowly decaying magnetic fields [42]. As a result, local inhomogeneity of the MR tomography main field can be originated, leading to the loss of phase coherence of the transversal component of the magnetization vector, and thus, rapid loss of image intensity in the area surrounding magnetic implants. These results suggest that, in the clinical use, Magnetic Resonance Imaging is not recommended for the surgical follow-up of a bone cement containing a ferrimagnetic glass ceramic in the amount investigated in this work.

4. Conclusions

In this work, bioactive and ferrimagnetic composite bone cements, based on a PMMA matrix containing bioactive and ferrimagnetic glass-ceramic particles, have been characterized in term of bioactivity, wettability, density, curing parameters, mechanical properties at 37 °C, with particular focus on the viscoelastic behaviour, the bending strengths and creep. Radiographic imaging (XR) and Magnetic

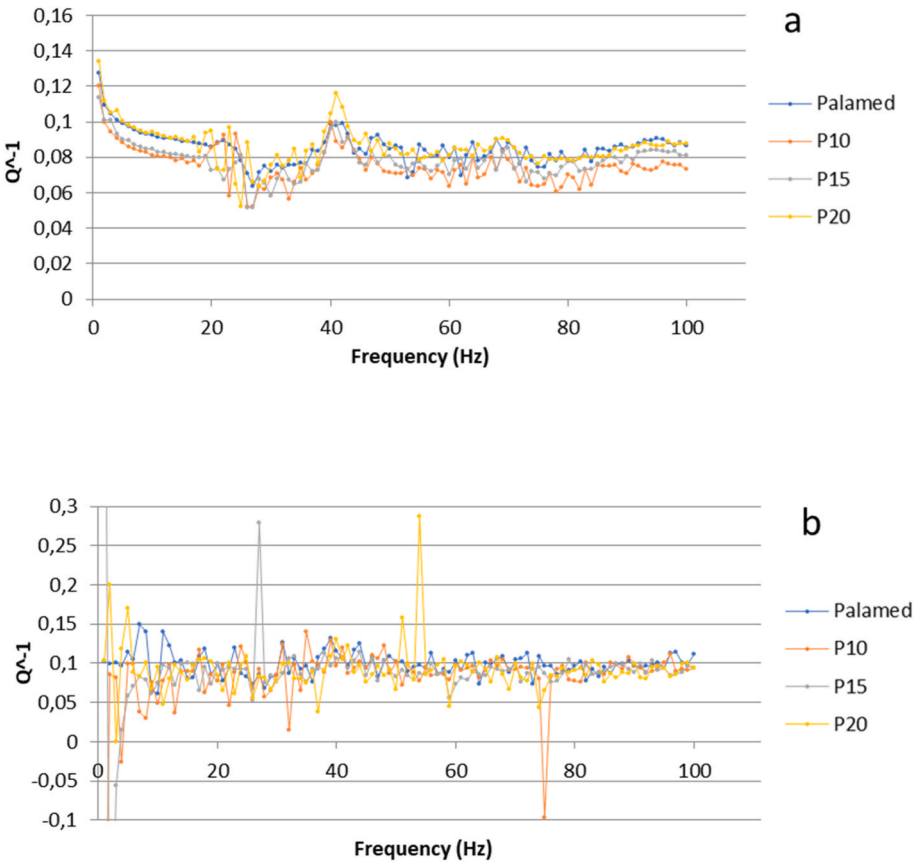

Fig. 7. Loss factor at room temperature (a) and at 37 °C (b).

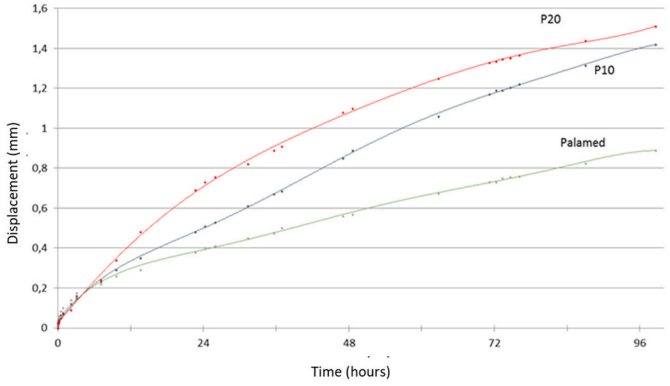

Fig. 8. Creep test (sample displacement vs. the time at 37 °C) for pure Palamed®, P10 and P20.

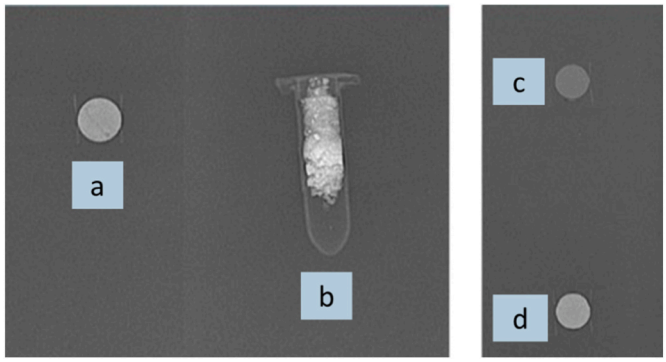

Fig. 9. Radiographies of the PMMA-based composite cements, without commercial radio-opaque phase, containing 20% SC45 glass-ceramic powders (a) compared with pure SC45 glass-ceramic powders (b) and a plain PMMA – based cement (same composition of the polymeric phase of Fig. 8a) without (c) and with (d) radiopaque phase.

Resonance Imaging (MRI) have been also performed in order to assess the possibility of performing *in vivo* clinical follow up. The ability of developing a layer of HA on the surface of the composite cements after immersion in SBF has been confirmed. The addition of the glass-ceramic filler in amount higher than 10% induced a wetting behaviour to the composite bone cements, that is expected to impart better osteointegration abilities. The curing parameters analysis revealed shorter curing times and lower maximum temperatures for the three composite cements in comparison to the plain one. The mechanical properties of the composite bone cements are almost unaffected in comparison to those of the plain commercial cement both at room and at 37 °C. In particular, only a few embrittlement in bending can be detected for glass-ceramic filler in amount higher than 15%, but any differences were perceptible on the fracture mechanism, from a morphological point of view, both at room and at 37 °C. Moreover, a little increase of the viscous flow has been evidenced in the composite samples at 37 °C due to the polymer softening induced by the temperature and, as a function of the glass ceramic particles amount, to the presence of porosity, as well as to a probable partial dissolution of the glass-ceramic particles during the tests performed in wet environment. The composite bone cements possess an intrinsic radiopacity with any image deformation, while MRI imaging causes strong image distortion, thus suggesting X-ray Imaging (XR) as the most suitable imaging technique, comparable to the previously investigated Computed Tomography (CT). Object of future investigations could be the assessment of the composite cements behaviour at the hyperthermia therapeutic conditions (i.e. 41 °C–43 °C).

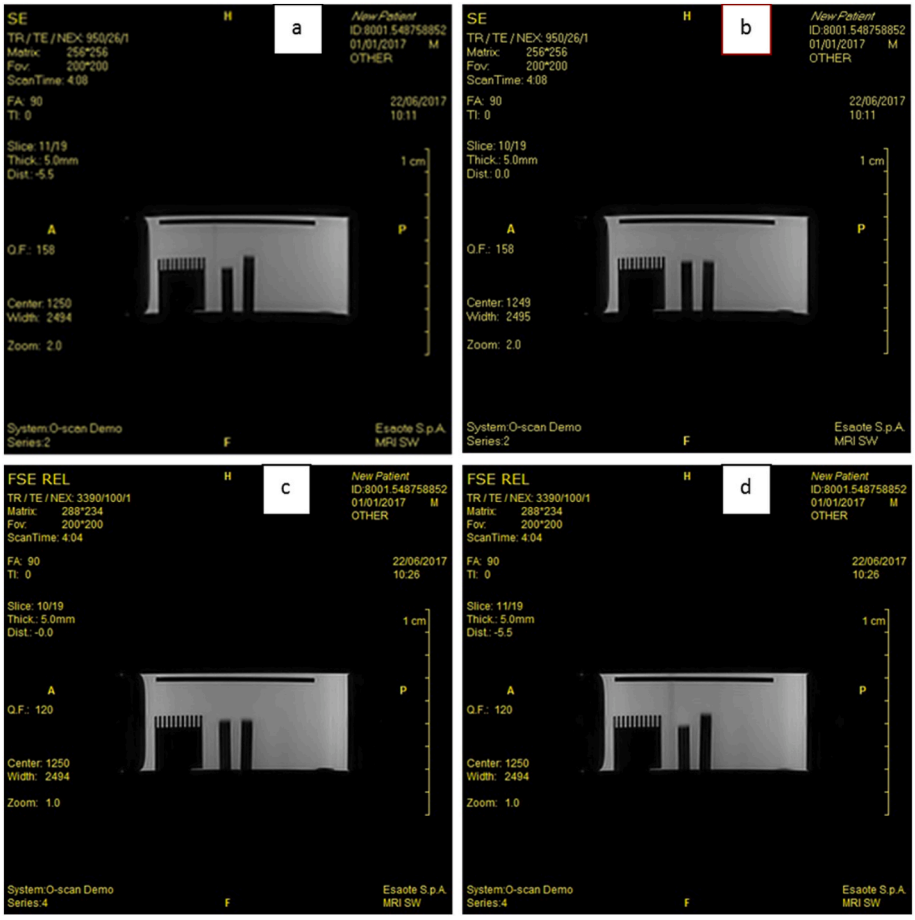

Fig. 10. *Spin-echo* scans of the phantom (central sections) containing the contrast liquid and the plain Palamed® samples weighted on T_1 (a, b) and T_2 (c, d).

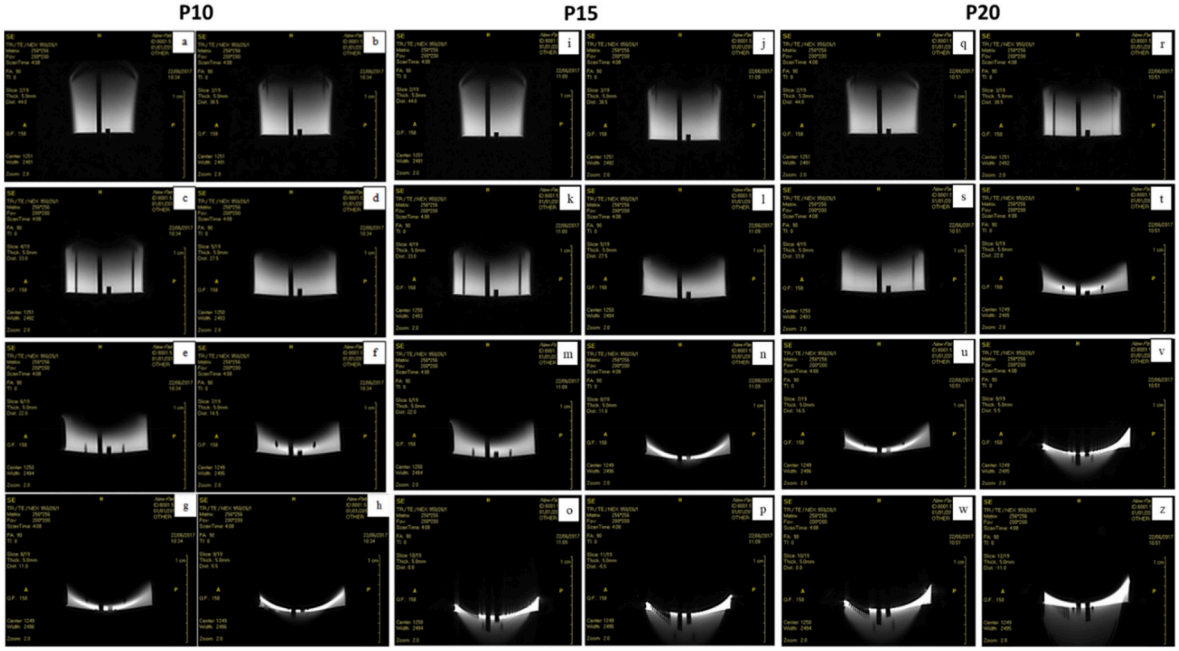

Fig. 11. *Spin-echo* scans of the phantom containing the contrast liquid and the composite bone cement samples weighted on T_1, in different sections, from surface to the central one (P10: a-h; P15: i-p; P20: q-z).

Declaration of competing interest

The authors declare that they have no known competing financial interests or personal relationships that could have appeared to influence the work reported in this paper.

Ackowledgements

The authors wish to thank the Radiology Unit of Istituto di Candiolo – Fondazione del Piemonte per l'Oncologia (FPO), IRCCS, Candiolo (Torino, Italy), for radiography facilities, and Sergio Paddeu, ESAOTE S. p.A., Genova ITALY, for Magnetic Resonance Imaging.

This research did not receive any specific grant from funding agencies in the public, commercial, or not-for-profit sectors.

References

[1] P. Moroz, S.K. Jones, B.N. Gray, Status of hyperthermia in the treatment of advanced liver cancer, J. Surg. Oncol. 77 (2001) 259–269, https://doi.org/10.1002/jso.1106.

[2] P. Wust, B. Hildebrandt, G. Sreenivasa, B. Rau, J. Gellermann, H. Riess, R. Felix, P. M. Schlag, Hyperthermia in combined treatment of cancer, Lancet Oncol. 3 (8) (2002) 487–497, https://doi.org/10.1016/S1470-2045(02)00818-5.

[3] A. Matsumine, K. Kusuzaki, T. Matsubara, K. Shintani, H. Satonaka, T. Wakabayashi, S. Miyazaki, K. Morita, K. Takegami, A. Uchida, Novel hyperthermia for metastatic bone tumors with magnetic materials by generating an alternating electromagnetic field, Clin. Exp. Metastasis 24 (2007) 191–200, https://doi.org/10.1007/s10585-007-9068-8.

[4] D. Chang, M. Lim, J.A.C.M. Goos, R. Qiao, Y.Y. Ng, F.M. Mansfeld, M. Jackson, T. P. Davis, M. Kavallaris, Biologically targeted magnetic hyperthermia: potential and limitations, Front. Pharmacol. 9 (2018) 831, https://doi.org/10.3389/fphar.2018.00831.

[5] M. Kusaka, K. Takegami, A. Sudo, T. Yamazaki, J. Kawamura, A. Uchida, Effect of hyperthermia by magnetite cement on tumor-induced bone destruction, J. Orthop. Sci. 7 (2002) 354–357, https://doi.org/10.1007/s007760200059.

[6] K. Takegami, T. Sano, H. Wakabayashi, J. Sonoda, T. Yamazaki, S. Morita, T. Shibuya, A. Uchida, New ferromagnetic bone cement for local hyperthermia, J. Biomed. Mater. Res. 43 (2) (1998) 210–214, https://doi.org/10.1002/(SICI)1097-4636(199822)43:2<210::AID-JBM16>3.0.CO;2-L.

[7] A. Portela, M. Vasconcelos, R. Branco, F. Gartner, M. Faria, J. Cavalheiro, An in vitro and in vivo investigation of the biological behavior of a ferrimagnetic cement for highly focalized thermotherapy, J. Mater. Sci. Mater. Med. 21 (2010) 2413–2423, https://doi.org/10.1007/s10856-010-4093-6.

[8] L.L. Hench, Bioceramics, J. Am. Ceram. Soc. 81 (1993) 705–1728, https://doi.org/10.1111/j.1151-2916.1998.tb02540.x.

[9] W. Cao, L.L. Hench, Bioactive materials, Ceram. Int. 22 (1996) 493–507, https://doi.org/10.1016/0272-8842(95)00126-3.

[10] O. Bretcanu, E. Verné, M. Cöisson, P. Tiberto, P. Allia, Magnetic properties of the ferrimagnetic glass-ceramics for hyperthermia, J. Magn. Magn Mater. 305 (2006) 529–533, https://doi.org/10.1016/j.jmmm.2006.02.264.

[11] O. Bretcanu, S. Spriano, E. Vernè, M. Coisson, P. Tiberto, P. Allia, The influence of crystallized Fe 3 O 4 on the magnetic properties of coprecipitation-derived ferrimagnetic glass-ceramic, Acta Biomater. 1 (2005) 421–429, https://doi.org/10.1016/j.actbio.2005.04.007.

[12] E. Verné, M. Miola, S. Ferraris, C.L. Bianchi, A. Naldoni, G. Maina, O. Bretcanu, Surface activation of a ferrimagnetic glass-ceramic for antineoplastic drugs grafting. Adv. Eng. Mater. 12(7):B309 - B319. https://doi.org/10.1002/adem.200980082.

[13] A. Cochis, M. Miola, O. Bretcanu, L. Rimondini, E. Vernè, Magnetic bioactive glass ceramics for bone healing and hyperthermic treatment of solid tumors, in: Ashutosh Tiwari et al. (Eds.), Advanced Magnetic and Optical Materials, Scrivener Publishing LLC ©, 2017, pp. 81–112.

[14] O. Bretcanu, M. Miola, C.L. Bianchi, I. Marangi, R. Carbone, I. Corazzari, M. Cannas, E. Verné, In vitro biocompatibility of a ferrimagnetic glass-ceramic for hyperthermia application, Mater. Sci. Eng. C. Mater . Biol. Appl. 73 (2017) 778–787, https://doi.org/10.1016/j.msec.2016.12.105.

[15] M. Miola, Y. Pakzad, S. Banijamali, S. Kargozar, C. Vitale-Brovarone, A. Yazdanpanah, O. Bretcanu, A. Ramedani, E. Vernè, M. Mozafari, Glass-ceramics for cancer treatment: so close, or yet so far? Acta Biomater. 83 (2019) 55–70, https://doi.org/10.1016/j.actbio.2018.11.013.

[16] M. Bruno, M. Miola, O. Bretcanu, C. Vitale-Brovarone, R. Gerbaldo, F. Laviano, E. Verné, Composite bone cements loaded with a bioactive and ferrimagnetic glass-ceramic: morphological, mechanical and calorimetric characterization, J. Biomater. Appl. 29 (2) (2014) 254–267, https://doi.org/10.1177/088532821452184, 29(2).

[17] E. Verné, M. Bruno, M. Miola, G. Maina, C. Bianco, A. Cochis, L. Rimondini, Composite bone cements loaded with a bioactive and ferrimagnetic glass-ceramic: leaching, bioactivity and cytocompatibility, Mater. Sci. Eng. C 53 (2015) 95–103, https://doi.org/10.1016/j.msec.2015.03.039.

[18] M. Miola, F. Laviano, R. Gerbaldo, M. Bruno, A. Lombardi, A. Cochis, L. Rimondini, E. Verné, Composite bone cements for hyperthermia: modeling and characterization of magnetic, calorimetric and in vitro heating properties, Ceram. Int. 43 (2017) 4831–4840, https://doi.org/10.1016/j.ceramint.2016.12.049.

[19] B. Pascual, B. Vàquez, M. Gurruchag, I. Goti, M.P. Ginebra, F.J. Gil, J.A. Planell, B. Levenfeld, J. San Romàn, New aspects of the effect of size and size distribution on the setting parameters and mechanical properties of acrylic bone cements, Biomaterials 17 (1996) 509–516, https://doi.org/10.1016/0142-9612(96)82725-6.

[20] B. Magnan, M. Bondi, T. Maluta, E. Samaila, L. Schirru, C. Dall'Oca, Acrylic bone cement: current concept review, Musculoskelet Surg 97 (2013) 93–100, https://doi.org/10.1007/s12306-013-0293-9.

[21] M.P. Ginebra, L. Albuixech, E. Fernàndez-Barragàn, C. Aparicio, F.J. Gil, J. San Romàn, B. Vàzquez, J.A. Planell, Mechanical performance of acrylic bone cements containing different radiopacifying agents, Biomaterials 23 (2002) 1873–1882, https://doi.org/10.1016/S0142-9612(01)00314-3.

[22] J.R. Frigstad, J.B. Park, Reinforcement of PMMA bone cement with a continuous wire coil–a 3D finite element study, Bio Med. Mater. Eng. 6 (1996) 429–439, https://doi.org/10.3233/BME-1996-6604.

[23] M. Beleani, L. Cristofolini, C. Minari, A. Toni, Fatigue strength of PMMA bone cement mixed with gentamicin and barium sulphate vs pure PMMA, J. Engineering in Medicine, Part H 217 (1) (2002) 9–12, https://doi.org/10.1243/095441103762597.

[24] M. Miola, G. Fucale, G. Maina, et al., Composites bone cements with different viscosities loaded with a bioactive and antibacterial glass, J. Mater. Sci. 52 (2017) 5133–5146, https://doi.org/10.1007/s10853-017-0750-1.

[25] M. Miola, A. Cochis, A. Kumar, C.R. Arciola, L. Rimondini, E. Verné, Cu-doped bioactive glass as filler for PMMA-based bone cements: morphological, mechanical, reactivity and preliminary antibacterial characterization, Materials 11 (6) (2018) 961, https://doi.org/10.3390/ma11060961.

[26] M.L. Parks, H.A. Walsh, E.A. Salvati, S. Li, Effect of increasing temperature on the properties of four bone cements, Clin. Orthop. Relat. Res. 355 (1998) 238–248.

[27] T. Kokubo, H. Takadama, How useful is SBF in predicting in vivo bone bioactivity? Biomaterials 27 (2006) 2907–2915, https://doi.org/10.1016/j.biomaterials.2006.01.017.

[28] C. Wu, Y. Xiao, Evaluation of the in vitro bioactivity of bioceramics, Bone Tissue Regen. Insights 2 (2009) 25–29, https://doi.org/10.4137/BTRI.S3188.

[29] S. Fujibayashi, M. Neo, H.M. Kim, T. Kokubo, T. Nakamura, A comparative study between in vivo bone ingrowth and in vitro apatite formation on Na_2O–CaO–SiO_2 glasses, Biomaterials 24 (2003) 1349–1356, https://doi.org/10.1016/S0142-9612(02)00511-2.

[30] T. Kokubo, Surface chemistry of bioactive glass-ceramics, J. Non-Cryst. Solids 120 (1990) 138–151, https://doi.org/10.1016/0022-3093(90)90199-V.

[31] R. Kumar Ranjan, M. Kumar, R. Kumar, M.F. Ali, Bone cements, International Journal of Orthopaedics Sciences 3 (4) (2017) 79–82, https://doi.org/10.22271/ortho.2017.v3.i4b.12.

[32] ISO 5833(2002) standard, Implants for Surgery- Acrylic Resin Cements.

[33] N. Verdonschot, R. Huiskes, Acrylic cement creeps but does not allow much subsidence of femoral stems, J Bone Joint Surg Br 79 (4) (1997) 665–669, https://doi.org/10.1302/0301-620x.79b4.7173. PMID: 9250762.

[34] E. Vernè, F. Foroni, G. Lucchetta, M. Miola, Antibacterial and bioactive composite bone cements, Current Materials Science 12 (2) (2019) 144–153, https://doi.org/10.2174/1874464812666190819143740.

[35] J.Y. Lim, M.C. Shaughnessy, Z. Zhou, H. Noh, E.A. Vogler, H.J. Donahue, Surface energy effects on osteoblast spatial growth and mineralization, Biomaterials 29 (12) (2008) 1776–1784, https://doi.org/10.1016/j.biomaterials.2007.12.026.

[36] Y. Zhang, O. Andrukhov, S. Berner, M. Matejka, M. Wieland, X. Rausch-Fan, A. Schedle, Osteogenic properties of hydrophilic and hydrophobic titanium surfaces evaluated with osteoblast-like cells (MG63) in coculture with human umbilical vein endothelial cells (HUVEC), Dent. Mater. 26 (11) (2010) 1043–1051, https://doi.org/10.1016/j.dental.2010.07.003.

[37] D. Gogola, A. Krafčík, O. Štrbák, I. Frollo, Magnetic resonance imaging of surgical implants made from weak magnetic materials, Meas. Sci. Rev. 13 (No. 4) (2013 165), https://doi.org/10.2478/msr-2013-0026.

[38] F. Kundie, C.H. Azhari, A. Muchtar, Z.A. Ahmad, Effects of filler size on the mechanical properties of polymer-filled dental composites: a review of recent developments, J. Physiol. Sci. 29 (1) (2018) 141–165, https://doi.org/10.21315/jps2018.29.1.10.

[39] M.P. Ginebra, C. Aparicio, L. Albuixech, E. Fernández-Barragán, F.J. Gil, J. A. Planell, Improvement of the mechanical properties of acrylic bone cements by substitution of the radio-opaque agent, J. Mater. Sci. Mater. Med. 10 (12) (1999) 733–737, https://doi.org/10.1023/A:1008979207968 PMID: 15347942.

[40] M. Baleani, M. Viceconti, The effect of adding 10% of barium sulphate radiopacifier on the mechanical behaviour of acrylic bone cement, Fatig. Fract. Eng. Mater. Struct. 34 (2010) 374–382.

[41] A. Sabokbar, Y. Fujikawa, D.W. Murray, N.A. Athanasou, Radio opaque agents in bone cement increase bone resorption, J. Bone Joint Surg. Br. 79 (1) (1997) 129–134, https://doi.org/10.1302/0301-620X.79B1.6966.

[42] D. Gogola, A. Krafčík, O. Štrbák, I. Frollo, Magnetic resonance imaging of surgical implants made from weak magnetic materials, Meas. Sci. Rev. 13 (4) (2013) 165, https://doi.org/10.2478/msr-2013-0026.